Achieving Air-Ground Communications in 802.11 Networks with Three-Dimensional Aerial Mobility

Evşen Yanmaz, Robert Kuschnig, and Christian Bettstetter
University of Klagenfurt, Lakeside Labs, Austria

***Abstract*—Increasing availability of autonomous small-size aerial vehicles leads to a variety of applications for aerial exploration and surveillance, transport, and other domains. Many of these applications rely on networks between aerial nodes, that will have high mobility dynamics with vehicles moving in all directions in 3D space and positioning in different orientations, leading to restrictions on network connectivity. In this paper, we propose a simple antenna extension to 802.11 devices to be used on aerial nodes. Path loss and small-scale fading characteristics of air-to-ground links are analyzed using signal strength samples obtained via real-world measurements at 5 GHz. Finally, network performance in terms of throughput and number of retransmissions are presented. Results show that a throughput of 12 Mbps can be achieved at distances in the order of 300 m.**

***Index Terms*—3D networks, 802.11, quadrotors, UAVs, vehicular communications, link modeling, Nakagami fading.**

I. Introduction

Applications in aerial environmental monitoring, border surveillance, object detection and tracking have led researchers to study the performance of wireless communications with nodes moving in three-dimensional (3D) space [1]–[4]. These applications require high performance links and connectivity in 3D with data delivery meeting quality of service demands.

The question arises as to which wireless technology should be employed for 3D mobility. A candidate is IEEE 802.11, due to its broad availability and the implementation of both infrastructure and ad-hoc modes to support a wide range of services. Network deployments of 802.11, however, generally assume communication on a 2D plane (e.g., a floor of a building), either for low mobility of people or high mobility of ground vehicles. Aerial networks, in turn, consist of air-ground and air-air links, and data needs to be delivered regardless of significant height and orientation differences. Directed antenna radiation characteristics are likely to have high impact on performance of 3D connectivity. This practical aspect is generally not included in theoretical analysis, where often isotropic or omnidirectional radiation is assumed.

In this work, we first discuss issues faced in communications in 3D space and propose a simple extension to off-the-shelf 802.11 systems with multiple antennas configured to fit on small-scale quadrocopters to address these issues. Second, we analyze via real-world measurements the path loss and fading characteristics of the radio channel between a flying quadrocopter and a ground station. In particular, we model the path loss exponent and parameters of Nakagami fading using received signal strength samples and verify 3D connectivity. To the best of our knowledge, there are no published results from measurement campaigns for such communication links besides our preliminary work [5]. The high data rates in 802.11 are enabled by techniques like adaptive rate control and link layer retransmissions, which are used to mitigate channel-related packet loss, but usually lead to high throughput fluctuations. As a result, applications need to adapt to varying throughput and limit the sensor data (e.g., video bit rate) to the available bandwidth. Thus, we also study network performance in terms of metrics such as throughput and number of retransmissions to observe if the 3D network is capable of supporting throughput and delay demands of applications of interest. Results show that our proposal can handle high movement dynamics, height and orientation differences, and provide high-throughput links in 3D space. The experimental results can be used in the implementation of new applications.

II. Related Work

A. Wireless Networks with Three-Dimensional Mobility

Initial research on 3D networks extends the theory of 2D networks without particular assumptions for deployed nodes [6], [7]. These works provide bounds for capacity, coverage, and connectivity of nodes placed in 3D shapes. With commercially available vehicles, more practical proposals are made, which deploy aerial networks for environmental and disaster monitoring, surveillance, search and rescue missions [1]–[3], [8]. In addition, 3D wireless ad hoc and sensor networks are analyzed, where a node, e.g., a single unmanned aerial vehicle (UAV), is used as relay or as mobile base station that collects data from the sensors, or multiple UAVs are used to create a communication chain between otherwise disconnected regions, where no infrastructure exists [9]–[11]. Several projects consider UAVs equipped with visual sensors to provide overview images of given areas or to detect and track objects with high link throughput demands [12], [13].

B. Link Measurements in UAV Networks

Measurements for UAVs with commercial wireless equipment can be found in the literature. In [14], the channel in air-to-air and air-to-ground communication is characterized for a network of micro-aerial vehicles equipped with 802.15.4 radios. In [1], throughput, connectivity, and range of a mesh network of ground and aerial vehicles equipped with 802.11b radios are measured. Impact of antenna orientations placed on a fixed wing UAV with 802.11a interface is illustrated via measurements on a linear flight path in [15].

III. Experimental System Setup

A. Aerial Vehicle and Communication System

We have chosen small-scale quadrocopters as our UAV system in our tests for their good maneuverability, ability

(a) Ubiquiti RouterStation (b) RouterStation and AscTec Pelican

Fig. 1. Experimental setup

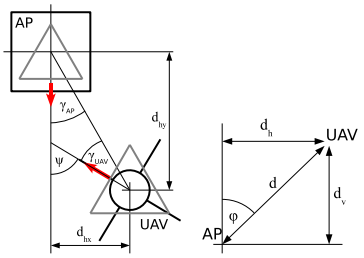

Fig. 2. Antenna configuration: Elevation, distances and angles.

to hover, and high mobility dynamics (such as tilt, roll, rotate). We use AscTec Pelican quadrocopters. The limited payload and processing power prevents installation of large communication infrastructure on board. As operating system, Ubuntu Linux kernel 3.2 is run on the UAV. The UAV is also equipped with a GPS and inertial measurement unit (IMU) module that provides the position and orientation.

The quadrocopter flies in the air and communicates via IEEE 802.11a wireless LAN to an access point (AP) at the ground. We have chosen 802.11a due to availability of high data rates and lower interference levels at 5.2 GHz compared to 2.4 GHz (which is used by the remote control). The wireless cards are configured to use the 802.11a channel 48 (5.240 GHz). A computer at the ground is used to control the measurements; it is connected via Ethernet to the AP. The AP consists of Ubiquiti's RouterStation and Ubiquiti SR71-A 802.11abgn mini-PCI module. The AP is put on a tripod and elevated to a height of approximately 3 m (see Fig. 1(a)). The 802.11abgn mini-PCIe module from SparkLAN WPEA-127N is used on the UAV. We conduct all the tests in an open field with no obstacles or clutter. The Linux-based OpenWRT operating system (kernel 3.2) is used on the AP.

The performance is measured using the Linux wireless subsystem [16], comprising the transmission rate, the received signal strength (RSS), and the number of retransmissions, among others. The test data is generated by a UDP packet generator (fixed UDP payload size of 1469 bytes), which fully utilizes the wireless network link. Different tests are conducted for the uplink (AP to UAV) and the downlink (UAV to AP), to assess the sending and receiving behavior.

B. Antennas

The radiated signal at a given direction is mainly affected by the radiation pattern and polarization of the antenna as well as by shielding caused by UAV hardware. In classical ground communications, omni-directional antennas in the azimuth plane, such as dipole antennas, can be sufficient to provide good connectivity. In three-dimensional UAV communications, however, there is a need for omni-directional radiation both in the azimuth and elevation planes (quasi-isotropic radiation).

Intuitively, multiple dipole antennas can be used to improve the three-dimensional characteristics of the antenna system. In [5], we show the performance of systems with two antennas and illustrate that it strongly depends on the orientation of the UAV to the ground station. The main reasons for that are the small overlap of the antenna beams and the high impact of polarization when aligning the antennas orthogonally, which leads to a high variation in the gain of the antenna system. To counter this, we increase the number of antennas used; to minimize the effects of polarization, we consider only antenna systems which are either horizontally or vertically aligned. Since horizontal antennas are easier to mount on UAVs, we use a triangular, horizontal three-antenna configuration, which we denote by HHH. Fig. 2 illustrates the configuration both on AP and UAV. We use Motorola ML-5299-APA1-01R dipole antennas with 2 dBi gain and 3 dB beamwidth of 360° and 75° in azimuth and elevation planes, respectively. Simple selection combining is done in the receiver, i.e., the antenna with the highest received signal strength (RSS) is chosen. Here, the three antennas are placed in such a manner that each antenna covers a third of the space (see gray rectangle in Fig. 2). A single vertical antenna setup (VV) is used as benchmark.

C. Location Conventions

The absolute position of UAV and AP are retrieved using the global positioning system (GPS). The absolute orientation to north (yaw) of the AP and the UAV is also measured. Using the absolute positions and yaw values of the AP and the UAV, a local coordinate system with the AP in the center can be constructed. Hence, the horizontal distance $d_h = \sqrt{d_{hx}^2 + d_{hy}^2}$ and the vertical distance d_v between the UAV and the AP can be calculated (see Fig. 2 for the convention and Fig. 1(b) for the antenna placement on the UAV and the router). The direct distance is given by $d = \sqrt{d_h^2 + d_v^2}$. Note that the heading of the AP and the UAV are marked with red arrows in the figure. The angle φ defines the elevation. The relative orientation (azimuth) of the AP to the UAV is defined by the angle γ_{AP}, while the relative orientation of the UAV to the AP is given by the angle γ_{UAV}. The angle $\psi = \gamma_{\text{AP}} + \gamma_{\text{UAV}}$ corresponds to the mismatch between the orientations of AP and UAV.

IV. Antenna Radiation Pattern

Our first test measures impact of the UAV's orientation on RSS. The location and orientation of the AP are fixed, where $\gamma_{\text{AP}} = 0$. The UAV holds its position at a fixed distance $d = 100$ m and elevation with $\varphi = 85°$, while the relative orientation of the UAV to the AP varies in 15° steps ($\gamma_{\text{UAV}} \in [0°, ..., 360°]$). Elevation level is chosen such that a fair comparison between VV and HHH setups can be done. Figure 3 shows the RSS (in dBm). To illustrate the antenna selection based on RSS level at each antenna for HHH antenna

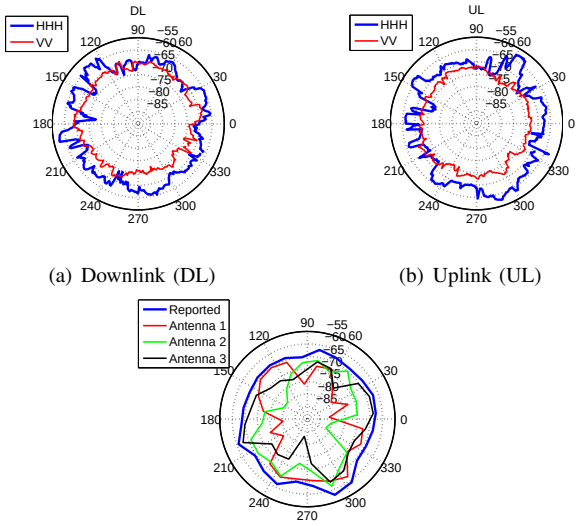

(a) Downlink (DL) (b) Uplink (UL)

(c) RSS from three antennas

Fig. 3. RSS in dBm versus γ_{UAV}, when $\varphi = 85°$, $\gamma_{\text{AP}} = 0°$, and $d = 100\,\text{m}$ (a) at AP and (b) at UAV, (c) at all antennas at UAV, smoothed in 15° bins.

setup, we also show the reception quality of the single antennas for the uplink test in Fig. 3(c). As expected, VV achieves an omni-directional radiation, with some fluctuation due to the mobility of the UAV and the environment (e.g., reflections from the ground or disturbances such as wind). The HHH setup also results in omni-directional radiation though with more fluctuations due to not only the mobility but also the radiation pattern of the antennas in the elevation plane. Both uplink (UL) and downlink (DL) tests result in similar performance. As shown in Fig. 3(c), the three antennas in triangle setup provide spatial diversity and share the space effectively. In this figure, we smooth the RSS values to better distinguish the *handoff* between the antennas. The reported value is obtained by averaging RSS shown in Fig. 3(b) in 15° bins.

Second, we investigate the impact of elevation of UAV on RSS for the two antenna setups, when $d = 100\,\text{m}$, $\gamma_{\text{AP}} = 0°$, and $\gamma_{\text{UAV}} = 0°$. Keeping distance fixed, elevation angle φ is changed in 5° steps within $[10°, 85°]$ (i.e., UAV ascends on the surface of a sphere). Results are shown in Fig. 4. Since the radiation pattern of a dipole is torus-shaped, on the elevation plane the VV setup suffers as φ decreases (i.e., as the UAV ascends on the sphere surface). The HHH setup, on the other hand, though affected by the radiation pattern of the specific antenna used in our tests can sustain a high RSS, achieving an omni-directional radiation in the elevation plane, hence eliminating impact of height differences between AP and UAV.

So far we have tested our setup with $\gamma_{\text{AP}} = 0°$. However, in real deployments of the UAV network, it is most likely that the relative orientation of the UAV with respect to the AP will change. Hence, third, we measure the RSS for the HHH setup in a scenario where the UAV moves around the AP, keeping a fixed distance $d = 111\,\text{m}$. For this scenario, the absolute orientation of the AP and the UAV are fixed to $\psi = 0°$, while γ_{AP} and γ_{UAV} naturally change. Figure 5 shows the RSS on the AP (DL) and UAV (UL) with respect to γ_{AP} for the test. Observe that the RSS in all relative positions to the AP sustain an average level of $-65\,\text{dBm}$ with a standard

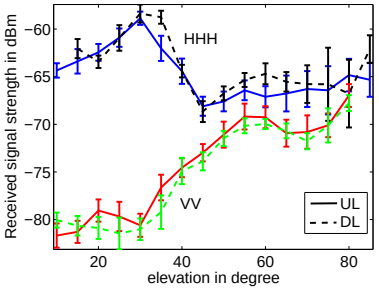

Fig. 4. RSS in dBm at UAV (UL) and AP (DL) versus UAV elevation φ in degree at $d = 100\,\text{m}$)

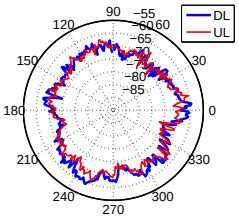

Fig. 5. RSS in dBm versus γ_{AP} in degree for the HHH antenna setup at $\varphi = 64°$, $\psi = 0°$, and $d = 111\,\text{m}$.

deviation of 2.5 dB for both UL and DL tests.

The results of this section illustrate the potential of a triangular antenna setup in 3D environments in terms of sustained connectivity. Such spherical radiation can intuitively eliminate the impact of horizontal and vertical displacements as well as different orientations.

V. Characterization of Aerial Links

A. Path Loss

To determine path loss parameters, we conduct tests over horizontal (d_h) and vertical (d_v) distances: (i)UAV flies away from or toward the AP on a straight line of length $d_h = 350\,\text{m}$ and at a fixed $d_v = 50\,\text{m}$; (ii) UAV ascends and descends over a straight line $d_v \in [20, 110]\,\text{m}$, at $d_h = 100\,\text{m}$ from the AP. Angles γ_{AP} and γ_{UAV} are fixed to 0°. Transmit power is set to 20 dBm. UAV travels on horizontal and vertical lines, stopping every 50 m and 20 m for 5 s, respectively. Since flights are conducted over open space without obstacles between AP and UAV, we adopt the log-distance path loss model:

$$\text{PL}(d) = \text{PL}(d_0) + 10\alpha \log_{10}\left(\frac{d}{d_0}\right) \quad (1)$$

where $\text{PL}(\cdot)$ is the path loss in dB at a given distance $d = \sqrt{d_h^2 + d_v^2}$, α is the path loss exponent, and d_0 is a reference distance. We assume the received signal undergoes free space propagation from the transmitter to d_0. Assuming antenna gains equal system losses, $d_0 = 1\,\text{m}$, the corresponding $\text{PL}(d_0)$ becomes 46.4 dB. We determine the minimum mean square error (MMSE) estimate of α using all measured values.

Figures 6(a) and 7(a) show the measured RSS on the uplink and downlink over distance for a horizontal line test, respectively, where the UAV flies away from the AP at $d_v = 50\,\text{m}$ height. The RSS samples measured over a horizontal distance of 20 m are shown in Fig. 6(c), marking the parts the UAV is on the move and it holds its position. Figures 6(b) and 7(b) show the measured RSS over distance for a vertical line test, where

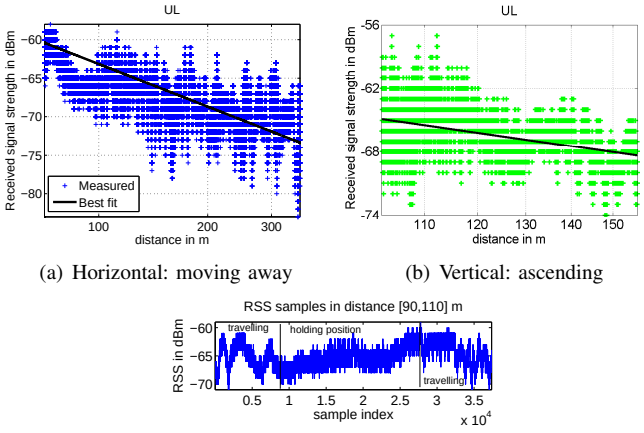

(a) Horizontal: moving away (b) Vertical: ascending

(c) Samples from horizontal line test

Fig. 6. RSS measured on the UL during the horizontal and vertical line tests.

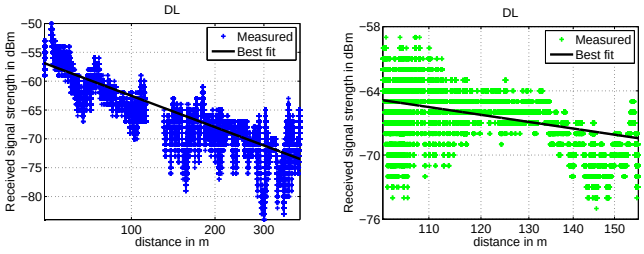

(a) Horizontal: moving away (b) Vertical: ascending

Fig. 7. RSS measured on DL during the horizontal and vertical line tests.

the UAV ascends at $d_h = 100\,\text{m}$, for uplink and downlink transmissions, respectively. The measured RSS in all cases are consistent with a signal undergoing distance-dependent path loss with an estimated average path loss exponent of $\alpha = 2.01$ regardless of the type of motion and orientation with respect to the access point.

We present the RSS between two flying UAVs over distance in Fig. 8. The results are collected in promiscuous mode, when two UAVs fly pre-computed paths at $d_v = 50\,\text{m}$ height and continuously transmit UDP traffic to the ground station. The relative orientation of the UAVs with respect to each other constantly changes. We observe that our proposed extension works successfully for UAV-UAV links as well (in both directions). The MMSE-estimate for path loss exponent is $\alpha = 2.03$.

B. Small-Scale Fading

As shown in Fig. 6(c), RSS of the UAV-to-ground link fluctuates due to multi-path fading and mobility of the UAV. Let us study next the fading statistics. For general scenarios, it is common practice to use Nakagami fading to characterize the wireless channel [17]. The probability density function (pdf) of the power of a signal undergoing Nakagami fading follows the Gamma distribution given by $\left(\frac{2m}{\Omega}\right)^m \frac{x^{m-1}}{\Gamma(m)} \exp[\frac{-2mx}{\Omega}]$ with parameters m and Ω. Given the measured signal power values P_i, $i = 1, ..., N$, we can determine the maximum likelihood estimates of these parameters using [18]:

$$\hat{\Omega} = \frac{2}{N}\sum_{i=1}^{N} P_i \quad \text{and} \quad \hat{m} = \frac{6 + \sqrt{36 + 48\Delta}}{24\Delta}, \tag{2}$$

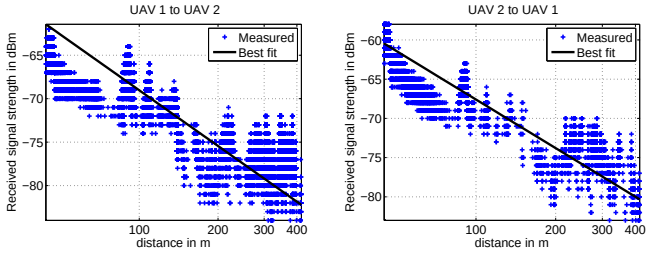

(a) (b)

Fig. 8. RSS measured on the UAV-UAV link during a waypoint flight test: (a) from UAV 1 to UAV 2 and (b) from UAV 2 to UAV 1.

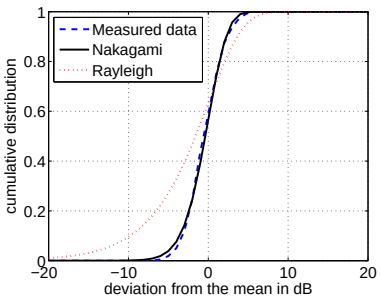

Fig. 9. CDF: RSS on DL (while UAV hovers)

where $\Delta = \log\left[\frac{2}{N}\sum_{i=1}^{N} P_i\right] - \frac{1}{N}\sum_{i=1}^{N}\log[2P_i]$. To determine the statistics of the UAV-ground channel, we analyze data from several scenarios; e.g., data measured when the UAV holds its position, or when the UAV is moving away from/toward the AP, or when UAV ascends/descends. Fig. 9 presents our results that correspond to the position hold test, where the UAV hovers at $d = 100\,\text{m}$ and $d_v = 15\,\text{m}$ for the DL test (results for UL are omitted due to limited space). The cumulative distribution function (CDF) of RSS from the measurements and theoretical distributions for Nakagami and Rayleigh fading are shown for comparison. Recall that Rayleigh fading is a special case of Nakagami fading with $m = 1$ and with parameter $\sigma = \sqrt{\frac{\Omega}{2}}$. The parameters of the distributions are estimated using (2), where P_i's are the measured RSS samples. For the position hold test, the estimated $\hat{\sigma}^2$ and $\hat{\Omega}/2$ are the average signal power around $-62\,\text{dBm}$ and $\hat{m} = 4.05$. While analyzing the data from moving tests, we first split the data into holding position and traveling sections. We then group the data received every $10\,\text{m}$ distance into a bin and determine the fading parameters for each bin. For the conducted horizontal and vertical line tests, we observe that Nakagami fading is a good fit for the measured RSS values collected during the travel phase of the tests as well. While $\hat{\Omega}$ can be estimated for each bin using (2) and it coincides with the estimated average received signal power at the corresponding distance (using the path loss from (1)), there is no unique $\hat{m}$ parameter value that spans all test distances. We only observe that $\hat{m}$ is always greater than 1, i.e., for these tests Rayleigh fading is not a good fit.

C. Network Performance

Finally, we present some network performance, where the UAV flies away from the AP and we focus on transmissions

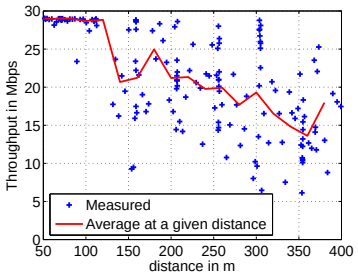

Fig. 10. UAV moving away: UDP throughput on the DL versus distance

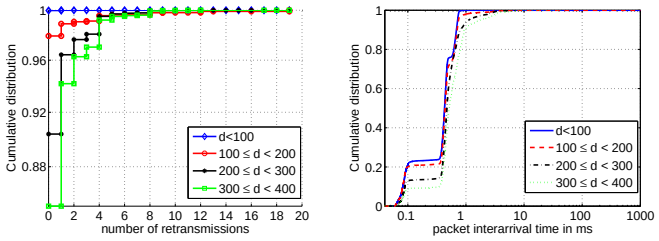

(a) CDF: number of retransmissions (b) CDF: packet inter-arrival time

Fig. 11. UAV moving away: CDFs of performance metrics

from the UAV to the AP (i.e., downlink). Since we have observed that the measured RSS follows similar tendencies for all tests, the presented results are also good performance indicators for the other scenarios studied in this paper. Fig. 10 shows the UDP throughput in Mbps over distance. We show both measured values and throughput averaged every 20 m. Since the UAV always has data to transmit, the results also show the link capacity. Observe that the average throughput gracefully degrades with distance in accordance with the rate adaptation mechanisms of the 802.11a standard. The instantaneous throughput changes at a given distance due to motion but on average high rates are sustained.

Fig. 11 shows the empirical CDFs of number of retransmissions and packet inter-arrival times for several distance intervals. The inter-arrival times and the number of retransmissions are measured at the receiver (i.e., AP) and the sender (i.e., UAV), respectively. These metrics in combination provide information on the achievable instantaneous throughput. Fig. 11(a) shows the CDF of the number of retransmissions at the link layer. Observe that even at the farthest range the number of retransmissions are at most 1 over 85% of the time, which is consistent with the high achieved rate and throughput. The packet inter-arrival time at the receiver is shown in Fig. 11(b). It can be noticed that for all distances the majority of the inter-arrival time is below 1 ms, resulting in an average throughput above 12 Mbps (compare also with Fig. 10). We also observe that 99 % and 99.9 % of the packets experience inter-arrival times of at most 3.47 ms and 7.73 ms, respectively. The corresponding minimum throughputs for these worst case inter-arrival times can be computed as 3.39 and 1.52 Mbps, respectively, when packet-payload is 1469 bytes.

VI. Conclusions and Further Work

This paper analyzed performance of 802.11 networks for dynamic 3D environments via real-world measurements. An experimental setup that consists of a ground station and small-scale quadrocopters has been used to realize 3D links. A simple extension to the communication system has been proposed to achieve quasi-isotropic radiation, providing uniform 3D-connectivity. We have tested the setup for several scenarios with different heights, orientations, and distances and have estimated the fading characteristics of the air-ground links. We have also measured the network performance. Our future work will focus on multiple-UAV networks and analyze UAV-UAV links as well as network throughput in more detail.

Acknowledgments

This work was funded by ERDF and KWF in the Lakeside Labs projects cDrones (grant 20214/17095/24772) and SINUS (grant 20214/24272/36084).

References

[1] T. X. Brown, B. Argrow, C. Dixon, S. Doshi, R. G. Thekkekunnel, and D. Henkel, "Ad hoc UAV ground network (Augnet)," in *Proc. AIAA Unmanned Unlimited Tech. Conf.*, Sept. 2004.

[2] M. Kovacina, D. Palmer, G. Yang, and R. Vaidyanathan, "Multi-agent control algorithms for chemical cloud detection and mapping using unmanned air vehicles," in *Proc. IEEE/RSJ Intl. Conf. on Intelligent Robots and Systems*, vol. 3, Oct. 2002, pp. 2782 – 2788.

[3] D. T. Cole, P. Thompson, A. H. Göktoğan, and S. Sukkarieh, "System development and demonstration of a cooperative UAV team for mapping and tracking," *Int. J. Rob. Res.*, vol. 29, pp. 1371–1399, Sep. 2010.

[4] A. Ryan, M. Zennaro, A. Howell, R. Sengupta, and J. Hedrick, "An overview of emerging results in cooperative UAV control," in *Proc. IEEE Conf. Decision and Control*, vol. 1, Dec. 2004, pp. 602 –607.

[5] E. Yanmaz, R. Kuschnig, and C. Bettstetter, "Channel measurements over 802.11a-based UAV-to-ground links," in *Proc. Intern. Workshop on Wireless Networking for Unmanned Autonomous Vehicles*, 2011.

[6] S. M. N. Alam and Z. J. Haas, "Coverage and connectivity in three-dimensional networks," in *Proc. Intl. Conf. Mobile Comp. and Net. (MOBICOM'06)*, 2006, pp. 346–357.

[7] P. Gupta and P. R. Kumar, "Internets in the sky: The capacity of three dimensional wireless networks," *Communications in Information and Systems*, vol. 1, pp. 33–50, 2001.

[8] P. Vincent and I. Rubin, "A framework and analysis for cooperative search using UAV swarms," in *Proc. ACM Symp. Appl. Comp.*, 2004.

[9] R. C. Palat, A. Annamalai, and J. H. Reed, "Cooperative relaying for ad hoc ground networks using swarms," in *Proc. IEEE Milit. Comm. Conf. (MILCOM'05)*, vol. 3, Oct. 2005, pp. 1588–1594.

[10] S. Hauert, J.-C. Zufferey, and D. Floreano, "Evolved swarming without positioning information: an application in aerial communication relay," *Autonomous Robots*, vol. 26, no. 1, 2009.

[11] D. Gu, G. Pei, H. Ly, M. Gerla, B. Zhang, and X. Hong, "UAV aided intelligent routing for ad-hoc wireless network in single-area theater," in *Proc. IEEE Wireless Commun. and Net. Conf.*, vol. 3, 2000.

[12] "Collaborative Microdrones [online]: http://www.cdrones.com/."

[13] L. Heng, G. H. Lee, F. Fraundorfer, and M. Pollefeys, "Real-time photo-realistic 3D mapping for micro aerial vehicles," in *IEEE/RSJ Intl. Conf. Intelligent Robots and Systems (IROS)*, Sept. 2011, pp. 4012 –4019.

[14] J. Allred, A. B. Hasan, S. Panichsakul, W. Pisano, P. Gray, J. Huang, R. Han, D. Lawrence, and K. Mohseni, "Sensorflock: an airborne wireless sensor network of micro-air vehicles," in *Proc. ACM Intl. Conf. Embedded Networked Sensor Systems (SENSYS'07)*, Nov. 2007.

[15] C.-M. Cheng, P.-H. Hsiao, H. Kung, and D. Vlah, "Performance measurement of 802.11a wireless links from UAV to ground nodes with various antenna orientations," in *Proc. Intl. Conf. Computer Comm. and Networks*, Oct. 2006, pp. 303 –308.

[16] R. Kuschnig, E. Yanmaz, I. Kofler, B. Rinner, and H. Hellwagner, "Profiling IEEE 802.11 Performance on Linux-based UAVs," in *Proc. Austrian Robotics Workshop (ARW'12)*, May 2012.

[17] J. D. Parsons, *The Mobile Radio Propagation Channel*. Wiley, 2000.

[18] J. Cheng and N. Beaulieu, "Maximum-likelihood based estimation of the Nakagami m parameter," *IEEE Commun. Lett.*, vol. 5, no. 3, pp. 101–103, March 2001.